THE JOURNAL OF PHYSICAL CHEMISTRY C
A JOURNAL OF THE AMERICAN CHEMICAL SOCIETY

pubs.acs.org/JPCC

Article

Chemical Characterization of a Three-Dimensional Double-Decker Molecule on a Surface via Scanning-Tunneling-Microscopy-Based Tip-Enhanced Raman Spectroscopy

Published as part of The Journal of Physical Chemistry virtual special issue "Nanophotonics for Chemical Imaging and Spectroscopy".

Sayantan Mahapatra, Jeremy F. Schultz, Linfei Li, Xu Zhang, and Nan Jiang*

Cite This: *J. Phys. Chem. C* 2022, 126, 8734–8741

Read Online

ACCESS | Metrics & More | Article Recommendations | Supporting Information

ABSTRACT: Three-dimensional double-decker building blocks (e.g., ferrocene or ferrocene-based molecules) hold great promise in molecular spintronics due to their built-in spin and charge functionality. However, despite this exciting prospect, chemical characterization of these molecules is rare. Herein, we investigate the self-organization of 1,1′-ferrocene dicarboxylic acid (FcDCA, $C_{12}H_{10}FeO_4$) on the Cu(100) surface using scanning tunneling microscopy (STM) and nonresonance tip-enhanced Raman spectroscopy (TERS). The experimental results are supplemented with density functional theory [DFT and time-dependent (TDDFT)] calculations. The combination of experimental and theoretical analyses provides the complete chemical characterization of FcDCA at the single-molecule level, as well as the chemical functionality of the carboxylic acid (−COOH) groups. The results here provide important chemical insight into double-decker organic molecules which is essential for device fabrication in next-generation electronics.

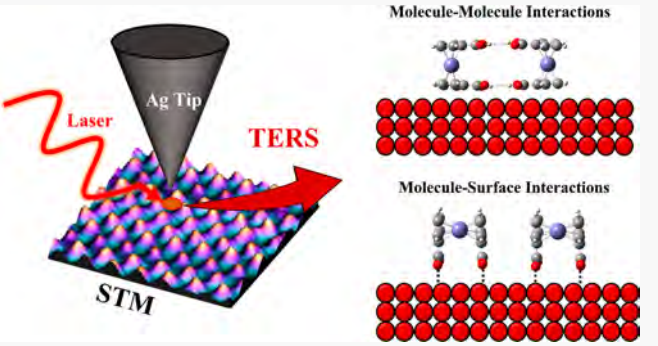

1. INTRODUCTION

Fundamental knowledge of the deposition, diffusion, growth mechanisms, and self-organized assembly formation of organic molecules on well-defined metal surfaces is of immense importance in many daily life applications including catalysis, biosensing, organic solar cells, as well as modern-day electronic devices with desirable optoelectronic properties.[1−5] Recognizing such on-surface processes relies on our understanding of the nature of fundamental surface-sensitive interactions, i.e., molecule−substrate and molecule−molecule interactions at the atomic level.[5−8] As a result, adsorption, desorption, molecular orientation, and self-assembled structure generation of specifically designed organic molecules have been investigated in recent years through a bottom-up approach.[9−11] For example, much effort has so far targeted the metallocene family of molecules [$M(C_5H_5)_2$, M = Co, Fe, etc.] on different coinage metal surfaces with scanning tunneling microscopy (STM) studies.[12−15] The realization of these three-dimensional double-decker molecular building blocks on metallic surfaces is likely to have diverse applications in molecular electronics and spintronics, nanomagnetism, and so forth.[16−18]

Although STM is capable of providing rich topographical insights into surface nanostructures, a more comprehensive (i.e., both structural and chemical) characterization of such surface systems with additional spectroscopic techniques is most desirable. In comparison to ensemble-averaged spectroscopic methods [e.g., X-ray photoelectron spectroscopy (XPS)], STM combined with tip-enhanced Raman spectroscopy (TERS) has been proven as a useful tool for complete surface characterization.[19−22] Due to the presence of the localized enhanced electromagnetic (EM) field at the plasmonically active tip apex, TERS is extremely sensitive to the molecules directly underneath the tip (near-field technique), enabling angstrom scale chemical characterization well below the diffraction limit of light.[19,23−25] Utilizing TERS, remarkable progress has been achieved in surface science applications ranging from biomolecules[26−31] and 2D-materials[32] to nanoscale catalytic processes.[33−36] Significantly, atomic-scale local interfacial strain with magnitudes as small

Received: February 28, 2022
Revised: April 13, 2022
Published: April 25, 2022

https://doi.org/10.1021/acs.jpcc.2c01434
J. Phys. Chem. C 2022, 126, 8734−8741

as 0.6% was recently discovered by TERS, validating it for interfacial characterization.[37]

In recent years, ferrocene-based molecules appear extremely promising due to their spin and charge functionality at the metal (Fe) core.[16,38] For example, ferrocene [Fc, $Fe(C_5H_5)_2$], a class of metallocene, usually remains stable when the central Fe atom stays at a +2 or +3 oxidation state. Therefore, these compounds can serve as an ideal candidate for the application of molecular spintronics, quantum cellular automata, and so forth.[39,40] Despite this exciting prospect, the chemical characterization of such metallocenes remains elusive up to now. On the other hand, carboxylic acids are typically incorporated because of their ability to form hydrogen bonding (C═O···OH type).[41,42] Additionally, carboxylic acid functional groups are biologically essential elements in cell membranes, proteins, amino acids, and metabolism. Therefore, it is extremely essential to study these acid groups' behavior and chemical stability in the presence of metal surfaces. The structural and chemical identification of FcDCA molecules and their self-assemblies on an atomically flat surface may potentially offer useful insights, which are important to future nanotechnological applications. In particular, these types of molecules with carboxylic acid functional groups can either form a strong hydrogen-bonded molecular network or experience chemical modification, depending on the underlying substrate and molecular functionality.[43]

In this article, we report our findings with ultrahigh vacuum (UHV) STM and nonresonance TERS measurements of 1,1′-ferrocene dicarboxylic acid (FcDCA), a ferrocene derivative that includes two carboxylic acids (−COOH) groups. We aim to clarify the adsorption process, self-assembly formation, and molecule-sensitive interactions (both molecule−molecule and molecule−substrate interactions) of FcDCA molecules deposited on a Cu(100) substrate under UHV conditions. By employing STM combined with nonresonance TERS and density functional theory (DFT), we can provide both structural and chemical characterization of the adsorption and three-dimensional molecular configuration as well as the self-assembly formation process.

2. EXPERIMENTAL AND THEORETICAL METHODS

Experiments were carried out in a variable temperature STM system (UNISOKU, USM1400) under a base pressure of 10^{-11} Torr. The Cu(100) single crystal sample was prepared in a preparation chamber (base pressure 1×10^{-10} Torr) which was separated from the STM chamber by a gate valve. The Cu(100) surface was cleaned via repeated cycles of Argon ion sputtering (1 kV, ~2.5×10^{-5} Torr) and indirect thermal annealing to 865 K. The FcDCA molecules (Figure 1a) were purchased from Millipore-Sigma (purity 96%) and sublimed onto the Cu(100) surface via a K-cell molecular evaporator (ACME Technology Co., Ltd.) for 1 min (100 °C) for submonolayer coverage. The sample was kept at room temperature during deposition. After that, the sample was transferred to the STM chamber for STM imaging and Raman spectroscopy experiments, which took place at liquid nitrogen temperature (78 K). Electrochemically etched Ag tips were used for STM imaging and TERS experiments.[44] The plasmonically active Ag tips were cleaned in the preparation chamber by Argon ion sputtering (1.5 kV, ~2.5×10^{-5} Torr) and used for STM and TERS experiments.[44]

A 633 nm continuous wave (cw) HeNe laser (LASOS) polarized parallel to the tip was utilized (incoming photon source) for the TERS experiments. The TERS signal was detected by an iso-plane SCT320 spectrograph (Princeton Instrument) combined with a Princeton Instrument PIXIS 100 CCD. The home-built optical setup has been illustrated in detail previously.[44] The UV−vis absorption spectrum was acquired via an Ocean Optics Red Tide spectrometer from an FcDCA solution (dissolved in DMF, ≈10^{-4} M) at 298 K.

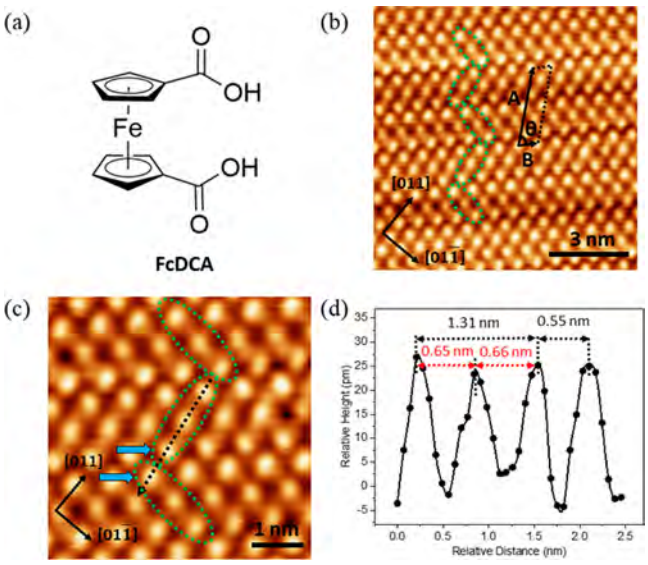

Figure 1. (a) Chemical structure of FcDCA. (b) Large-scale constant-current STM image of FcDCA on the Cu(100) surface. The "zig-zag"-type pattern is denoted using a few green dotted ellipsoids. The unit cell is marked by a black parallelogram. (c) STM image (zoom-in) of FcDCA island where the green dotted ellipsoids are used to show the "zig-zag" pattern. (d) Relative height profile along the black dotted arrow in (c), showing the lateral distance (1.31 nm) of three bright features inside a green dotted ellipsoid. The lateral distance between two other bright features (marked using two cyan arrows in (c)) is measured as 0.55 nm.

DFT calculations were performed using the VASP package[45] with the projector augmented wave pseudopotentials[46] and the Perdew−Burke−Ernzerhof gradient approximation.[47] The van der Waals (vdW) interaction was corrected with a nonlocal correlation functional.[48,49] An energy cutoff of 400 eV was used for the plane-wave basis set. Only the Γ-point in the Brillouin zone was used considering the large size of the supercell. We employed a four-layer slab with a (5 × 5) unit cell for the Cu(100) surface. The atoms in the top two layers were fully relaxed while the rest of the atoms were fixed in the equilibrium positions. The force convergence criterion for atomic relaxation is 0.01 eV/Å. The vibrational modes of the adsorbed FcDCA were obtained in the presence of the Cu(100) surface (which are kept frozen) by solving the eigenvalue problems of a dynamical or Hessian matrix based on density functional theory calculations.[50] Time-dependent DFT (TDDFT)[51] calculations were employed to determine the Raman intensity of the FcDCA molecules with the adsorption configuration. Note that the approximation by freezing the Cu surface in the spectra calculation could result in the shift of some Raman peaks compared to experimental TERS, which will be discussed in the following.

3. RESULTS AND DISCUSSION

3.1. Scanning Tunneling Microscopy. Long-range, compact molecular islands of FcDCA on the Cu(100) surface

https://doi.org/10.1021/acs.jpcc.2c01434
J. Phys. Chem. C 2022, 126, 8734−8741

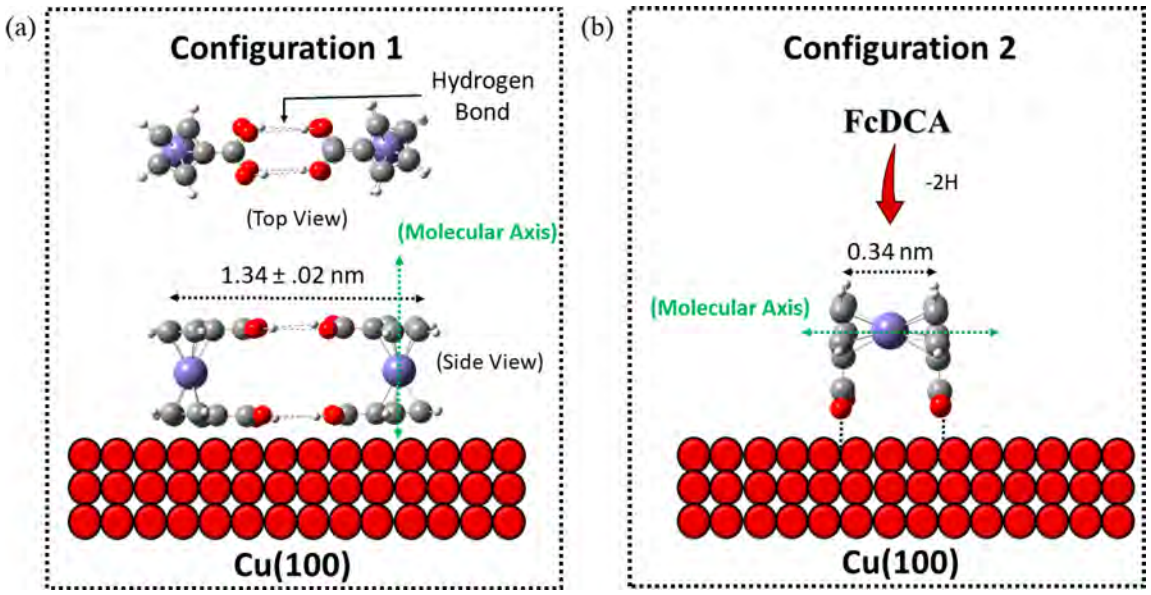

Figure 2. (a) Speculated Configuration 1. The FcDCA molecules can adsorb vertically (molecular axis perpendicular to the Cu surface) to form a hydrogen-bonded dimer (top-view and side-view). Considering the hydrogen bond length of 2.90 ± 0.2 Å, the dimer model provides a length of 1.34 ± 0.02 nm. (b) Speculated Configuration 2. The FcDCA molecules can adsorb horizontally (molecular axis parallel to the Cu surface) after losing two hydrogens. The deprotonated-FcDCA provides a length of 0.34 nm for a single molecule.

can be visualized in constant-current STM imaging (Supporting Information, Figure S1). The molecular structure appears to be stable as the FcDCA molecules are significantly constrained by the neighboring molecules, leading to a well-ordered structure formation, as shown in Figure 1b. The unit cell of the molecular self-organized assembly is marked with a black parallelogram (Figure 1b). The corresponding unit cell vectors are $\vec{A}$ = 2.93 ± 0.02 nm and $\vec{B}$ = 0.72 ± 0.03 nm and the angle between the vectors is θ = 75 ± 2°. Careful inspection (Figure 1b and c) reveals a "zig-zag"-type pattern structure (as marked by a few green ellipses in Figure 1b and c), distributed across the self-organized network. Figure 1d shows a line profile obtained in the direction of the black dotted arrow in Figure 1c. As shown, the lateral distance between the two bright features located at the edge of the two separate green dotted ellipses (marked by two cyan arrows in Figure 1c) is measured as 0.55 ± 0.01 nm. However, inside the green dotted ellipse, the lateral distance obtained between two bright features is slightly larger (i.e., 0.65 ± 0.02 nm), showing a total distance of 1.31 ± 0.03 nm across the three bright protrusions (inside one ellipse).

In an earlier STM study of basic ferrocene (Fc) molecules on the Cu(100) and Cu(111) substrates at liquid helium temperature (4.5 K), the molecules within a 2D molecular arrangement were argued to adopt two distinct types of configurations, that is, vertical- and horizontal-lying structure, depending on the orientation of cyclopentadienyl (Cp) rings.[12] Quite similar adsorption configurations (i.e., "standing-up" and "lying-down") were also observed for FcDCA molecules on the Ag(111) and Au(111) substrates, where the carboxylic acid functional groups are involved in strong hydrogen bonding for the "standing-up" configuration, thereby leading to the formation of dimers.[43] On the other hand, chemical modification, i.e., dehydrogenation of the −COOH groups, was reported to be the dominant process for adsorption on Cu(110) and Cu_3N/Cu(110) substrates.[43] In addition to STM measurements, their interpretations of FcDCA molecular configurations on different surfaces relied upon surface spectroscopic techniques, e.g., X-ray photoemission/near-edge X-ray absorption fine structure (XPS/NEXAFS) measurements.[43] Although such spectroscopic techniques hint toward multiple configurations, they lack spatially resolved characterization since they are ensemble-averaged measurements.

STM measurements have been proven to offer preliminary interpretations about the intermolecular and molecule−substrate interactions. If the molecular system is planar, larger, and aromatic, STM imaging remains adequate in visualizing the internal structures of the molecule, as well as intermolecular features.[52,53] STM images reveal the complicated electronic structure of the adsorbed molecule by probing the local density of states (LDOS). As a consequence, conclusive determination of adsorption configurations from STM images may experience some issues, particularly, if the molecule is particularly small or nonplanar. In this experiment on the Cu(100) substrate, we attempted tentative configuration assignments of the adsorbed FcDCA molecules. Based on these previous studies, we focused on both possibilities on the Cu(100) surface, i.e., strong intermolecular interactions to form a hydrogen-bonded dimer as well as strong molecule−substrate interactions to drive molecular deprotonation, as shown in Figure 2.

Let us first concentrate on the analysis of the hydrogen-bonded dimer formation case (Configuration 1). FcDCA molecules can adsorb vertically [molecular axis (defined in Figure 2a) perpendicular to the surface] with their Cp rings in an eclipsed conformation, thereby forming strong hydrogen bonds through the acid groups (C═O···OH) with another FcDCA molecule to generate a dimeric structure (Figure 2a). Considering the hydrogen bond distance of 2.9 ± 0.2 Å between the acid groups,[54] this dimer-FcDCA model provides a length of 1.34 ± 0.02 nm (Figure 2a), comparable to the experimental length (1.31 ± 0.03 nm) based on the measured lateral distances of three bright protrusions (Figure 1d). Therefore, two FcDCA molecules (i.e., dimer) could

https://doi.org/10.1021/acs.jpcc.2c01434
J. Phys. Chem. C 2022, 126, 8734−8741

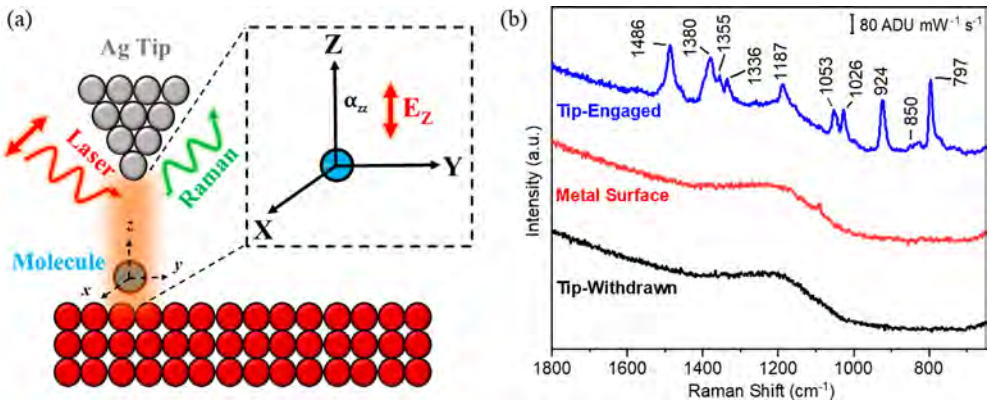

Figure 3. (a) Schematic illustration of TERS selection rules. The incident laser radiation (polarized parallel to the Ag tip) induces an intense and confined electromagnetic field within the STM nanogap. The frame of reference of the molecule and the coordinates of the enhanced plasmon field (mainly oriented in the *z*-direction) is displayed inside the dashed box. The molecular coordinates are labeled as *x*, *y*, and *z* using the black dotted arrow. (b) TERS fingerprint (blue) of FcDCA molecule when the tip is parked (and engaged) over molecular island. The tip-engaged spectrum over the metal surface (red) and the tip-retracted spectrum (black) is featureless. λ_{ex} = 633 nm, P_{acq} = 0.5 mW, t_{acq} = 5 s.

correspond to three bright features (inside one green dotted ellipse) in the STM image. On the other hand, strong interactions with the surface of the FcDCA molecule could lead to horizontal adsorption (molecular axis parallel to the surface, Figure 2b), indicating the molecules bind to the Cu(100) substrate using both carboxylate (−COO) groups with four O−Cu bonds (Configuration 2), as shown in the Figure 2b. This deprotonated adsorption configuration produces a length of ∼0.34 nm for a single molecule (Figure 2b). Therefore, the three bright features in the STM image could also be correlated with three deprotonated-FcDCA molecules.

As shown, one cannot thoroughly discern between these two tentative configurations (Configurations 1 and 2) for FcDCA self-assembly on Cu(100) substrate as both of the lateral lengths fit relatively well to the experiment and appear equally probable. Significantly, the lateral distance is composed of three more or less similar bright features. Considering the possibility of the FcDCA molecules making a hydrogen-bonded dimer, one could argue that the hydrogen-bonded area will be less in apparent height compared to the other parts of the molecule. However, this brightness does not necessarily correspond to the real height or topography, as it is sensitive to the frontier molecular orbital near the Fermi level (LDOS), as previously mentioned. Therefore, the bright features (i.e., relative heights) in the STM image could vary for the same object depending on the applied bias, tip conditions, molecular adsorption sites, and so forth. Thus, the formation of a three-bright structure in the STM image could become possible either from two FcDCA molecules (such as a dimer) or three deprotonated FcDCA molecules. Due to the lack of sufficient intermolecular resolution, the STM imaging alone appears to be insufficient to provide conclusive evidence to properly identify the configuration and self-assembled structure of FcDCA molecules on the Cu(100) surface, requiring another sophisticated surface-sensitive spectroscopic technique.

3.2. Nonresonance Tip-Enhanced Raman Spectroscopy. Although STM is a very powerful surface characterization technique, it lacks chemical sensitivity. In the previous report, spectroscopic techniques were utilized for FcDCA molecules in order to provide a logical interpretation of the STM images.[43] However, following the STM imaging of a particular molecular self-assembled area, nanoscale spectroscopic information on the same molecules can provide local chemical information, leading to a one-to-one correspondence with previously obtained STM images (i.e., both topographical and chemical information on the same surface area). In that sense, STM-TERS appears to be an effective tool to probe the surface structure locally.[55−58] Focusing the laser light at the tip−sample junction, the detection of the enhanced Raman fingerprint of a single molecule becomes attainable.[59−61] Recently, vibrational normal Raman modes of a single molecule adsorbed on a Cu(100) surface have been visualized using TERS.[24] Furthermore, it appears feasible to identify these two FcDCA configurations (i.e., vertical- and horizontal-lying configurations) with their molecular axes perpendicular to each other using TERS selection rules. Since the laser light is polarized parallel to the tip axis, components of the enhanced EM field parallel to the tip axis are dominant compared to the perpendicular components.[62,63] Thus, out-of-plane vibrational modes (*z*-components) of a molecule are more likely to be enhanced compared to the in-plane modes (*x*-, *y*-components) as they match the orientation of the plasmonic field (Figure 3a).[64,65] Therefore, we supplement our STM-based results with TERS, providing the complete chemical characterization of FcDCA on the Cu(100) substrate.

When the incident photon energy is close in energy to the electronic transition [from the highest occupied molecular orbital (HOMO) to the lowest unoccupied molecular orbital (LUMO)] of the molecular system, the frequency coincidence can provide greatly enhanced intensity in the Raman scattering process (a phenomenon known as resonance Raman effect).[66,67] This process also facilitates the chemical analysis of surface adsorbed molecular systems with single molecule sensitivity. Recently, angstrom scale chemical characterization has been demonstrated for the chemical identification of two porphodilactone isomers by resonant TERS in the visible region with a red laser [633 nm (1.95 eV), for better coincidence with the last Q-band of porphodilactone molecules].[68] However, when the same 633 nm laser excitation is employed for the FcDCA molecules with the optical absorption (HOMO to LUMO excitation) mainly in the early visible region [441 nm (2.81 eV), Supporting Information, Figure S2], the Raman process becomes nonresonant. In comparison to the resonance Raman process, nonresonance Raman scattering is weak which makes it challenging to resolve

https://doi.org/10.1021/acs.jpcc.2c01434
J. Phys. Chem. C 2022, 126, 8734−8741

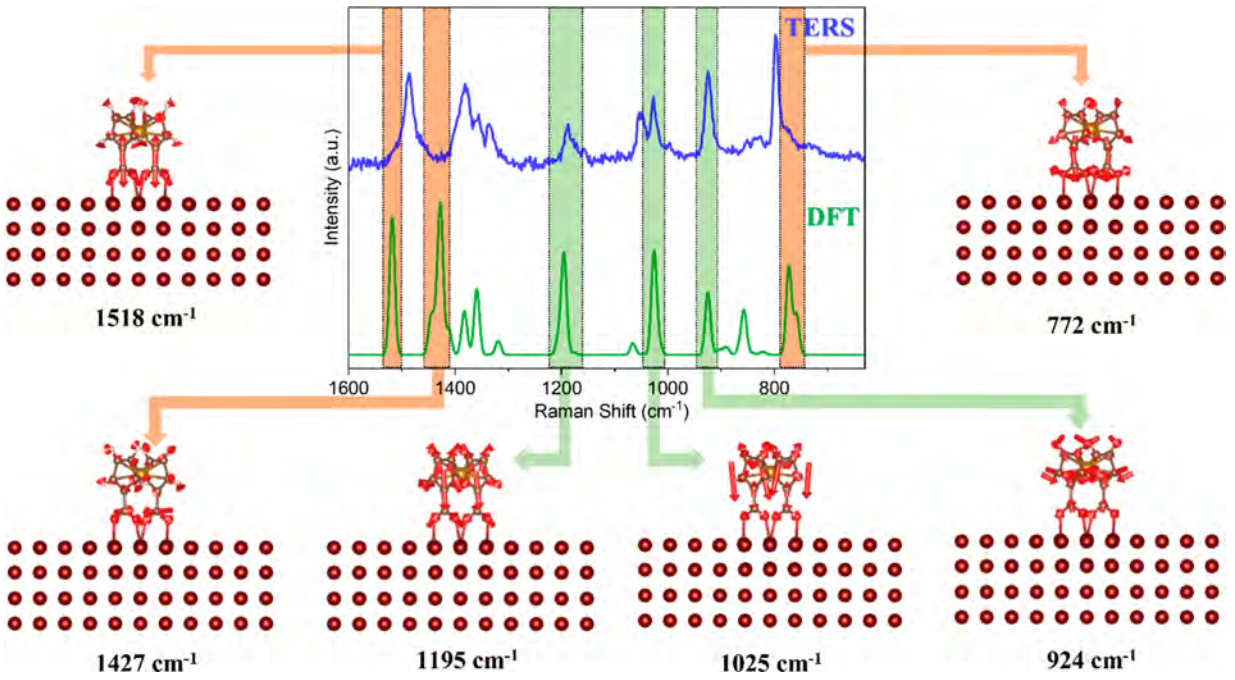

Figure 4. Comparison between simulated TERS (*z*-direction, green spectrum) for horizontal-lying FcDCA [adsorbed on Cu(100)] and experimental TERS (blue spectrum). Vibrational modes of significantly shifted peaks (highlighted in light orange color) and closely matched peaks (highlighted in light green color). The corresponding wavenumbers are assigned accordingly.

molecular structure.[69] Our work, presented here, reports the detection of multiple discrete enhanced Raman peaks of the adsorbed FcDCA molecules (Figure 3b, blue spectrum) when the tip was engaged (and parked) over the molecular island. Such enhancement of Raman signal is attributed to the unique design of our chamber and optical setup, described in detail in our previous publications.[44,67] In comparison, the tip-engaged spectrum on the bare metal surface (Figure 3b, red spectrum) or the tip-retracted spectrum (Figure 3b, black spectrum) appears featureless, providing evidence that the Ag tip is not contaminated during the experiment and the amplified Raman signal originates from the molecules underneath the tip.

To gain a complete understanding of the experimental TERS spectrum of FcDCA and the corresponding binding configuration, we performed DFT and TDDFT calculations. First, we carried out DFT simulations to obtain the energetically favorable structure of both the speculated vertical- and horizontal-lying configurations (i.e., Configurations 1 and 2) of FcDCA on the Cu(100) surface. Then, we computed the nonresonance Raman spectra of the two configurations based on TDDFT calculations and compared them to the nonresonance TERS results of FcDCA in terms of both the positions and relative intensities of vibrational modes. The simulated spectra were separated into *x*-, *y*-, and *z*-components (Supporting Information, Figure S3), and specifically the *z*-components (out-of-plane vibrational modes) of vertical- and horizontal-lying configurations were compared with the experimental TERS spectrum based on the expected effects of the selection rules of TERS, as mentioned previously. As shown in the Supporting Information (Figure S4b), the spectral mismatch is apparent when we align the experimental TERS and the calculated TERS spectrum of Configuration 1. In contrast to the featureless behavior in the 1800−1600 cm^{-1} region (in the experiment), the simulated spectrum identifies the presence of strong peaks, corresponding to carboxylic acid (−COOH) functional groups. Furthermore, a significant spectral mismatch is evident in other spectroscopic regions also, providing conclusive evidence that the FcDCA cannot be adsorbed in the speculated fashion (i.e., Configuration 1). After that, in order to realize whether strong surface interaction leads to the deprotonation of FcDCA molecules (i.e., Configuration 2), we align the simulated Raman spectrum of deprotonated FcDCA adsorbed on Cu(100) with the experimental TERS spectrum. As seen in Figures 4 and S4d, most of the prominent peaks in the calculated spectrum can be closely matched with the experimental TERS spectrum (in terms of intensity and wavenumber), except the 1600−1450 cm^{-1} region which will be discussed later. Thus, out of the two possible configurations, we confirm the rapid surface-driven deprotonation process as a governing process for the FcDCA molecules on the Cu(100) surface, resulting in the adsorption of the FcDCA molecules with a dipodal-type interaction via both the carboxylate groups. In combination with the (TD)DFT simulations, the nonresonant TERS results provide the molecular binding configuration in three dimensions. The FcDCA molecules adsorb on the Cu(100) surface horizontally in an eclipsed fashion (in the bridge sites on the metal surface), losing two hydrogen atoms. Meanwhile, the carboxylate groups provide strong chemical interaction (σ-bonds) with the underlying Cu atoms with four equivalent Cu−O distances (d_{Cu-O} = 1.97 Å), as observed on the Cu(110) surface.[43]

Although most of the dominant peaks in our simulated Raman spectrum can find their counterparts in the experimental deprotonated FcDCA species TERS spectrum, one notable exception is the 1600−1450 cm^{-1} spectral region, specifically the 1518 and 1427 cm^{-1} peaks (Figure 4). These two peaks appear to experience a significant shift compared to the experimental TERS spectrum, whereas the other vibrational modes, e.g., 1195 or 924 cm^{-1}, closely match with the experiment. In addition, the 772 cm^{-1} peak also experiences a

https://doi.org/10.1021/acs.jpcc.2c01434
J. Phys. Chem. C 2022, 126, 8734−8741

moderate shifting. If one takes a closer look at these shifted vibrational modes as well as the closely matched vibrational modes (Figures 4 and S5), it is quite evident that the 1518 and 1427 cm^{-1} peaks (or the 772 cm^{-1} peak) are dominated by the vibrations of the carboxylate (−COO) groups which are strongly bonded to the underlying Cu atoms. Whereas, for other closely matched peaks, e.g., 1195, 1025, and 924 cm^{-1}, the vibrational modes are dominated by vibrations of the ferrocene structure. As the Cu atoms were kept frozen during the phonon simulation, the 1518 and 1427 cm^{-1} vibrational modes are likely to be more susceptible to frequency shifts than others due to the strong σ-bonding interactions between Cu atoms of the underlying Cu(100) surface and the oxygen atoms of the carboxylate (−COO) groups in this binding configuration.

After the binding configuration of a single FcDCA molecule has been confirmed by TERS, we now propose a tentative model for the self-assembled monolayer on the Cu(100) surface, based on the STM image (Figure 5). Three-bright

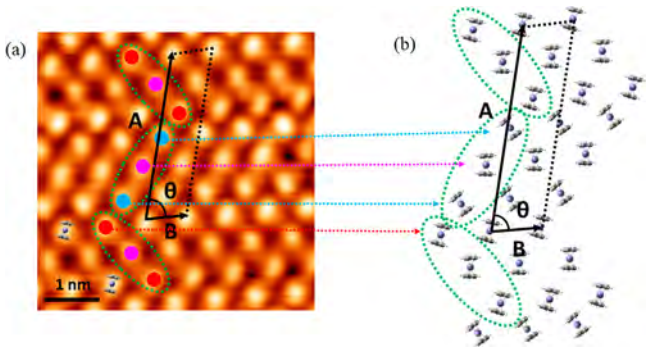

Figure 5. (a) STM image of the FcDCA self-assembly. The unit cell parameters (i.e., $\vec{A}$, $\vec{B}$, and θ) are marked using a black parallelogram. Each colored circle (red, pink, and cyan) represents one horizontally lying FcDCA molecule. The same color represents molecules of the same orientation while a different color suggests that the molecule experiences a rotation around z-axis. (b) Proposed self-assembled structure. The unit cell parameters (i.e., $\vec{A}$, $\vec{B}$, and θ) are marked using a black parallelogram.

protrusions in the STM image (inside the green dotted ellipse, Figure 5a) correspond to three FcDCA molecules adsorbed horizontally. In addition, careful inspection reveals topographical differences between the bright features in the STM image, which can be associated with molecular rotation around the z-axis.[43] The individual molecules are marked by light blue, red, and pink circles in Figure 5a, where the same-colored circles define molecules with the same orientation and different colored circles represent different orientations (i.e., molecular rotation around the z-axis). Based on the STM image, a tentative model of the scaled deprotonated-FcDCA self-assembly is proposed in Figure 5b, where the unit cell vectors (i.e., $\vec{A}$, $\vec{B}$, and θ) are marked. Various types of intermolecular interactions between the hydrogen atoms of the Cp ring as well as the η^5-coordination center of the Cp ring can be possible in this self-assembly, as can be seen in the model. However, due to poor intermolecular resolution obtained in the STM image, we cannot completely rule out other scenarios, where different types of intermolecular interactions can exist inside the molecular network.

4. CONCLUSION

Taken all together, the adsorption configuration of FcDCA molecules on the Cu(100) substrate has been explored by UHV-STM and nonresonance TERS in combination with DFT and TDDFT calculations. Two types of discrete molecular configurations, i.e., vertical- and horizontal-lying configurations, can be proposed based on the STM images. Both of the configurations are argued to fit well with the STM experiment; therefore, both are considered as possible candidates. Finally, the chemical fingerprints attained using TERS display a crucial sensitivity to the molecular orientation and binding configuration, confirming the horizontal-lying configuration for FcDCA on the Cu(100) surface. The fine agreement between the experimental and simulated Raman spectra suggests that the molecules experience rapid surface-driven deprotonation during deposition, leading to a dipodal-type chemisorption structure with the underlying substrate via the carboxylate groups (four equivalent Cu−O interactions). In the case of such double-decker organic molecules, the growth of a self-organized assembly over a solid surface depends on the characterization of local chemical effects at the atomic scale. STM-TERS is shown here as an ideal tool to probe the adsorbed configuration of these three-dimensional double-decker molecular structures that are essential for next-generation device fabrication.

■ ASSOCIATED CONTENT

Supporting Information

The Supporting Information is available free of charge at https://pubs.acs.org/doi/10.1021/acs.jpcc.2c01434.

Ball and stick model of FcDCA and large-scale STM image of self-assembled structure; UV−vis absorption spectra of FcDCA dissolved in dimethylformamide (DMF) at 298 K; simulated nonresonance Raman spectra of FcDCA molecule in Configurations 1 and 2 on the Cu(100) surface in the x-, y-, and z-directions; comparison between experimental and calculated spectra (z-direction) for Configurations 1 and 2; zoom-in views of vibrational normal modes (PDF)

■ AUTHOR INFORMATION

Corresponding Author

Nan Jiang − *Department of Chemistry, University of Illinois Chicago, Chicago, Illinois 60607, United States;* orcid.org/0000-0002-4570-180X; Email: njiang@uic.edu

Authors

Sayantan Mahapatra − *Department of Chemistry, University of Illinois Chicago, Chicago, Illinois 60607, United States;* orcid.org/0000-0002-7332-196X

Jeremy F. Schultz − *Department of Chemistry, University of Illinois Chicago, Chicago, Illinois 60607, United States;* orcid.org/0000-0003-2231-6797

Linfei Li − *Department of Chemistry, University of Illinois Chicago, Chicago, Illinois 60607, United States;* orcid.org/0000-0002-5217-3005

Xu Zhang − *Department of Physics and Astronomy, California State University, Northridge, California 91330, United States;* orcid.org/0000-0002-6491-3234

Complete contact information is available at: https://pubs.acs.org/10.1021/acs.jpcc.2c01434

https://doi.org/10.1021/acs.jpcc.2c01434
J. Phys. Chem. C 2022, 126, 8734−8741

Notes

The authors declare no competing financial interest.

■ ACKNOWLEDGMENTS

N.J. acknowledges support from the National Science Foundation (CHE-1944796). X.Z. acknowledges support from the National Science Foundation (DMR-1828019).

■ REFERENCES

(1) De Feyter, S.; De Schryver, F. C. Two-Dimensional Supramolecular Self-Assembly Probed by Scanning Tunneling Microscopy. *Chem. Soc. Rev.* **2003**, *32*, 139−150.
(2) Elemans, J. A. A. W.; van Hameren, R.; Nolte, R. J. M.; Rowan, A. E. Molecular Materials by Self-Assembly of Porphyrins, Phthalocyanines, and Perylenes. *Adv. Mater.* **2006**, *18*, 1251−1266.
(3) Whitelam, S. Examples of Molecular Self-Assembly at Surfaces. *Adv. Mater.* **2015**, *27*, 5720−5725.
(4) Hoeben, F. J. M.; Jonkheijm, P.; Meijer, E. W.; Schenning, A. P. H. J. About Supramolecular Assemblies of Π-Conjugated Systems. *Chem. Rev.* **2005**, *105*, 1491−1546.
(5) Bouju, X.; Mattioli, C.; Franc, G.; Pujol, A.; Gourdon, A. Bicomponent Supramolecular Architectures at the Vacuum−Solid Interface. *Chem. Rev.* **2017**, *117*, 1407−1444.
(6) Chiang, N.; Jiang, N.; Madison, L. R.; Pozzi, E. A.; Wasielewski, M. R.; Ratner, M. A.; Hersam, M. C.; Seideman, T.; Schatz, G. C.; Van Duyne, R. P. Probing Intermolecular Vibrational Symmetry Breaking in Self-Assembled Monolayers with Ultrahigh Vacuum Tip-Enhanced Raman Spectroscopy. *J. Am. Chem. Soc.* **2017**, *139*, 18664−18669.
(7) Bartels, L. Tailoring Molecular Layers at Metal Surfaces. *Nat. Chem.* **2010**, *2*, 87−95.
(8) Stepanow, S.; Lingenfelder, M.; Dmitriev, A.; Spillmann, H.; Delvigne, E.; Lin, N.; Deng, X.; Cai, C.; Barth, J. V.; Kern, K. Steering Molecular Organization and Host−Guest Interactions Using Two-Dimensional Nanoporous Coordination Systems. *Nat. Mater.* **2004**, *3*, 229−233.
(9) Ohtake, T. Bottom-up Approaches for Material and Device Designing Using Practical Aspects of Self-Assembled Molecular Architectures. *Mol. Syst. Des. Eng.* **2018**, *3*, 804−818.
(10) Kim, F. S.; Ren, G.; Jenekhe, S. A. One-Dimensional Nanostructures of Π-Conjugated Molecular Systems: Assembly, Properties, and Applications from Photovoltaics, Sensors, and Nanophotonics to Nanoelectronics. *Chem. Mater.* **2011**, *23*, 682−732.
(11) Li, L.; Mahapatra, S.; Liu, D.; Lu, Z.; Jiang, N. On-Surface Synthesis and Molecular Engineering of Carbon-Based Nanoarchitectures. *ACS Nano* **2021**, *15*, 3578−3585.
(12) Ormaza, M.; Abufager, P.; Bachellier, N.; Robles, R.; Verot, M.; Le Bahers, T.; Bocquet, M.-L.; Lorente, N.; Limot, L. Assembly of Ferrocene Molecules on Metal Surfaces Revisited. *J. Phys. Chem. Lett.* **2015**, *6*, 395−400.
(13) Garnier, L.; Verlhac, B.; Abufager, P.; Lorente, N.; Ormaza, M.; Limot, L. The Kondo Effect of a Molecular Tip as a Magnetic Sensor. *Nano Lett.* **2020**, *20*, 8193−8199.
(14) Wasio, N. A.; Quardokus, R. C.; Forrest, R. P.; Lent, C. S.; Corcelli, S. A.; Christie, J. A.; Henderson, K. W.; Kandel, S. A. Self-Assembly of Hydrogen-Bonded Two-Dimensional Quasicrystals. *Nature* **2014**, *507*, 86−89.
(15) Brown, R. D.; Coman, J. M.; Christie, J. A.; Forrest, R. P.; Lent, C. S.; Corcelli, S. A.; Henderson, K. W.; Kandel, S. A. Evolution of Metastable Clusters into Ordered Structures for 1,1′-Ferrocenedicarboxylic Acid on the Au(111) Surface. *J. Phys. Chem. C* **2017**, *121*, 6191−6198.
(16) Heinrich, B. W.; Limot, L.; Rastei, M. V.; Iacovita, C.; Bucher, J. P.; Djimbi, D. M.; Massobrio, C.; Boero, M. Dispersion and Localization of Electronic States at a Ferrocene/Cu(111) Interface. *Phys. Rev. Lett.* **2011**, *107*, 216801.
(17) Morari, C.; Rungger, I.; Rocha, A. R.; Sanvito, S.; Melinte, S.; Rignanese, G.-M. Electronic Transport Properties of 1,1′-Ferrocene Dicarboxylic Acid Linked to Al(111) Electrodes. *ACS Nano* **2009**, *3*, 4137−4143.
(18) Ormaza, M.; Robles, R.; Bachellier, N.; Abufager, P.; Lorente, N.; Limot, L. On-Surface Engineering of a Magnetic Organometallic Nanowire. *Nano Lett.* **2016**, *16*, 588−593.
(19) Mahapatra, S.; Li, L.; Schultz, J. F.; Jiang, N. Tip-Enhanced Raman Spectroscopy: Chemical Analysis with Nanoscale to Angstrom Scale Resolution. *J. Chem. Phys.* **2020**, *153*, 010902.
(20) Pozzi, E. A.; Goubert, G.; Chiang, N.; Jiang, N.; Chapman, C. T.; McAnally, M. O.; Henry, A.-I.; Seideman, T.; Schatz, G. C.; Hersam, M. C.; et al. Ultrahigh-Vacuum Tip-Enhanced Raman Spectroscopy. *Chem. Rev.* **2017**, *117*, 4961−4982.
(21) Verma, P. Tip-Enhanced Raman Spectroscopy: Technique and Recent Advances. *Chem. Rev.* **2017**, *117*, 6447−6466.
(22) Jiang, N.; Foley, E. T.; Klingsporn, J. M.; Sonntag, M. D.; Valley, N. A.; Dieringer, J. A.; Seideman, T.; Schatz, G. C.; Hersam, M. C.; Van Duyne, R. P. Observation of Multiple Vibrational Modes in Ultrahigh Vacuum Tip-Enhanced Raman Spectroscopy Combined with Molecular-Resolution Scanning Tunneling Microscopy. *Nano Lett.* **2012**, *12*, 5061−5067.
(23) Zhang, R.; Zhang, Y.; Dong, Z. C.; Jiang, S.; Zhang, C.; Chen, L. G.; Zhang, L.; Liao, Y.; Aizpurua, J.; Luo, Y.; et al. Chemical Mapping of a Single Molecule by Plasmon-Enhanced Raman Scattering. *Nature* **2013**, *498*, 82−86.
(24) Lee, J.; Crampton, K. T.; Tallarida, N.; Apkarian, V. A. Visualizing Vibrational Normal Modes of a Single Molecule with Atomically Confined Light. *Nature* **2019**, *568*, 78−82.
(25) Bhattarai, A.; Joly, A. G.; Hess, W. P.; El-Khoury, P. Z. Visualizing Electric Fields at Au(111) Step Edges Via Tip-Enhanced Raman Scattering. *Nano Lett.* **2017**, *17*, 7131−7137.
(26) Paulite, M.; Blum, C.; Schmid, T.; Opilik, L.; Eyer, K.; Walker, G. C.; Zenobi, R. Full Spectroscopic Tip-Enhanced Raman Imaging of Single Nanotapes Formed from B-Amyloid(1−40) Peptide Fragments. *ACS Nano* **2013**, *7*, 911−920.
(27) He, Z.; Han, Z.; Kizer, M.; Linhardt, R. J.; Wang, X.; Sinyukov, A. M.; Wang, J.; Deckert, V.; Sokolov, A. V.; Hu, J.; et al. Tip-Enhanced Raman Imaging of Single-Stranded DNA with Single Base Resolution. *J. Am. Chem. Soc.* **2019**, *141*, 753−757.
(28) Helbing, C.; Deckert-Gaudig, T.; Firkowska-Boden, I.; Wei, G.; Deckert, V.; Jandt, K. D. Protein Handshake on the Nanoscale: How Albumin and Hemoglobin Self-Assemble into Nanohybrid Fibers. *ACS Nano* **2018**, *12*, 1211−1219.
(29) Alexander, K. D.; Schultz, Z. D. Tip-Enhanced Raman Detection of Antibody Conjugated Nanoparticles on Cellular Membranes. *Anal. Chem.* **2012**, *84*, 7408−7414.
(30) Wang, H.; Schultz, Z. D. Ters Detection of Avβ3 Integrins in Intact Cell Membranes. *Chem. Phys. Chem.* **2014**, *15*, 3944−3949.
(31) Xiao, L.; Bailey, K. A.; Wang, H.; Schultz, Z. D. Probing Membrane Receptor−Ligand Specificity with Surface- and Tip-Enhanced Raman Scattering. *Anal. Chem.* **2017**, *89*, 9091−9099.
(32) Sheng, S.; Wu, J.-b.; Cong, X.; Li, W.; Gou, J.; Zhong, Q.; Cheng, P.; Tan, P.-h.; Chen, L.; Wu, K. Vibrational Properties of a Monolayer Silicene Sheet Studied by Tip-Enhanced Raman Spectroscopy. *Phys. Rev. Lett.* **2017**, *119*, 196803.
(33) Schultz, J. F.; Mahapatra, S.; Li, L.; Jiang, N. The Expanding Frontiers of Tip-Enhanced Raman Spectroscopy. *Appl. Spectrosc.* **2020**, *74*, 1313−1340.
(34) Zhong, J.-H.; Jin, X.; Meng, L.; Wang, X.; Su, H.-S.; Yang, Z.-L.; Williams, C. T.; Ren, B. Probing the Electronic and Catalytic Properties of a Bimetallic Surface with 3 Nm Resolution. *Nat. Nanotechnol.* **2017**, *12*, 132−136.
(35) Su, H.-S.; Feng, H.-S.; Zhao, Q.-Q.; Zhang, X.-G.; Sun, J.-J.; He, Y.; Huang, S.-C.; Huang, T.-X.; Zhong, J.-H.; Wu, D.-Y.; et al. Probing the Local Generation and Diffusion of Active Oxygen Species on a Pd/Au Bimetallic Surface by Tip-Enhanced Raman Spectroscopy. *J. Am. Chem. Soc.* **2020**, *142*, 1341−1347.
(36) Xiao, L.; Schultz, Z. D. Spectroscopic Imaging at the Nanoscale: Technologies and Recent Applications. *Anal. Chem.* **2018**, *90*, 440−458.

https://doi.org/10.1021/acs.jpcc.2c01434
J. Phys. Chem. C 2022, 126, 8734−8741

(37) Li, L.; Schultz, J. F.; Mahapatra, S.; Liu, X.; Shaw, C.; Zhang, X.; Hersam, M. C.; Jiang, N. Angstrom-Scale Spectroscopic Visualization of Interfacial Interactions in an Organic/Borophene Vertical Heterostructure. *J. Am. Chem. Soc.* **2021**, *143*, 15624−15634.
(38) García-Suárez, V. M.; Ferrer, J.; Lambert, C. J. Tuning the Electrical Conductivity of Nanotube-Encapsulated Metallocene Wires. *Phys. Rev. Lett.* **2006**, *96*, 106804.
(39) Lent, C. S.; Tougaw, P. D.; Porod, W.; Bernstein, G. H. Quantum Cellular Automata. *Nanotechnology* **1993**, *4*, 49−57.
(40) Orlov, A. O.; Amlani, I.; Bernstein, G. H.; Lent, C. S.; Snider, G. L. Realization of a Functional Cell for Quantum-Dot Cellular Automata. *Science* **1997**, *277*, 928−930.
(41) Quardokus, R. C.; Wasio, N. A.; Brown, R. D.; Christie, J. A.; Henderson, K. W.; Forrest, R. P.; Lent, C. S.; Corcelli, S. A.; Alex Kandel, S. Hydrogen-Bonded Clusters of 1, 1′-Ferrocenedicarboxylic Acid on Au(111) Are Initially Formed in Solution. *J. Chem. Phys.* **2015**, *142*, 101927.
(42) Yadav, K.; Mahapatra, S.; Halbritter, T.; Heckel, A.; Gopakumar, T. G. Low-Threshold Reversible Electron-Induced and Selective Photoinduced Switching of Azobenzene Derivatives under Ambient Conditions. *J. Phys. Chem. Lett.* **2018**, *9*, 6326−6333.
(43) Berger, J.; Kośmider, K.; Stetsovych, O.; Vondráček, M.; Hapala, P.; Spadafora, E. J.; Švec, M.; Jelínek, P. Study of Ferrocene Dicarboxylic Acid on Substrates of Varying Chemical Activity. *J. Phys. Chem. C* **2016**, *120*, 21955−21961.
(44) Mahapatra, S.; Li, L.; Schultz, J. F.; Jiang, N. Methods to Fabricate and Recycle Plasmonic Probes for Ultrahigh Vacuum Scanning Tunneling Microscopy-Based Tip-Enhanced Raman Spectroscopy. *J. Raman Spectrosc.* **2021**, *52*, 573−580.
(45) Kresse, G.; Furthmüller, J. Efficient Iterative Schemes for Ab Initio Total-Energy Calculations Using a Plane-Wave Basis Set. *Phys. Rev. B* **1996**, *54*, 11169−11186.
(46) Blöchl, P. E. Projector Augmented-Wave Method. *Phys. Rev. B* **1994**, *50*, 17953−17979.
(47) Perdew, J. P.; Burke, K.; Ernzerhof, M. Generalized Gradient Approximation Made Simple. *Phys. Rev. Lett.* **1996**, *77*, 3865−3868.
(48) Dion, M.; Rydberg, H.; Schröder, E.; Langreth, D. C.; Lundqvist, B. I. Van Der Waals Density Functional for General Geometries. *Phys. Rev. Lett.* **2004**, *92*, 246401.
(49) Klimeš, J.; Bowler, D. R.; Michaelides, A. Van Der Waals Density Functionals Applied to Solids. *Phys. Rev. B* **2011**, *83*, 195131.
(50) Baroni, S.; de Gironcoli, S.; Dal Corso, A.; Giannozzi, P. Phonons and Related Crystal Properties from Density-Functional Perturbation Theory. *Rev. Mod. Phys.* **2001**, *73*, 515−562.
(51) Zhang, X. Large-Scale Ab Initio Calculations of Raman Scattering Spectra within Time-Dependent Density Functional Perturbation Theory. *J. Chem. Phys.* **2018**, *148*, 244103.
(52) Jiang, N.; Zhang, Y. Y.; Liu, Q.; Cheng, Z. H.; Deng, Z. T.; Du, S. X.; Gao, H. J.; Beck, M. J.; Pantelides, S. T. Diffusivity Control in Molecule-on-Metal Systems Using Electric Fields. *Nano Lett.* **2010**, *10*, 1184−1188.
(53) Sk, R.; Deshpande, A. Unveiling the Emergence of Functional Materials with Stm: Metal Phthalocyanine on Surface Architectures. *Mol. Syst. Des. Eng.* **2019**, *4*, 471−483.
(54) Griessl, S.; Lackinger, M.; Edelwirth, M.; Hietschold, M.; Heckl, W. M. Self-Assembled Two-Dimensional Molecular Host-Guest Architectures from Trimesic Acid. *Single Mol.* **2002**, *3*, 25−31.
(55) Tallarida, N.; Rios, L.; Apkarian, V. A.; Lee, J. Isomerization of One Molecule Observed through Tip-Enhanced Raman Spectroscopy. *Nano Lett.* **2015**, *15*, 6386−6394.
(56) El-Khoury, P. Z. Tip-Enhanced Raman Scattering on Both Sides of the Schrödinger Equation. *Acc. Chem. Res.* **2021**, *54*, 4576−4583.
(57) El-Khoury, P. Z.; Schultz, Z. D. From Sers to Ters and Beyond: Molecules as Probes of Nanoscopic Optical Fields. *J. Phys. Chem. C* **2020**, *124*, 27267−27275.
(58) Schultz, J. F.; Li, L.; Mahapatra, S.; Jiang, N. Chemically Imaging Nanostructures Formed by the Covalent Assembly of Molecular Building Blocks on a Surface with Ultrahigh Vacuum Tip-Enhanced Raman Spectroscopy. *J. Phys.: Condens. Matter* **2022**, *34*, 204008.
(59) Jaculbia, R. B.; Imada, H.; Miwa, K.; Iwasa, T.; Takenaka, M.; Yang, B.; Kazuma, E.; Hayazawa, N.; Taketsugu, T.; Kim, Y. Single-Molecule Resonance Raman Effect in a Plasmonic Nanocavity. *Nat. Nanotechnol.* **2020**, *15*, 105−110.
(60) Jiang, S.; Zhang, Y.; Zhang, R.; Hu, C.; Liao, M.; Luo, Y.; Yang, J.; Dong, Z.; Hou, J. G. Distinguishing Adjacent Molecules on a Surface Using Plasmon-Enhanced Raman Scattering. *Nat. Nanotechnol.* **2015**, *10*, 865−869.
(61) Li, L.; Schultz, J. F.; Mahapatra, S.; Lu, Z.; Zhang, X.; Jiang, N. Chemically Identifying Single Adatoms with Single-Bond Sensitivity During Oxidation Reactions of Borophene. *Nat. Commun.* **2022**, *13*, 1796.
(62) Jiang, N.; Chiang, N.; Madison, L. R.; Pozzi, E. A.; Wasielewski, M. R.; Seideman, T.; Ratner, M. A.; Hersam, M. C.; Schatz, G. C.; Van Duyne, R. P. Nanoscale Chemical Imaging of a Dynamic Molecular Phase Boundary with Ultrahigh Vacuum Tip-Enhanced Raman Spectroscopy. *Nano Lett.* **2016**, *16*, 3898−3904.
(63) Schultz, J. F.; Li, L.; Mahapatra, S.; Shaw, C.; Zhang, X.; Jiang, N. Defining Multiple Configurations of Rubrene on a Ag(100) Surface with 5 Å Spatial Resolution Via Ultrahigh Vacuum Tip-Enhanced Raman Spectroscopy. *J. Phys. Chem. C* **2020**, *124*, 2420−2426.
(64) Shao, F.; Dai, W.; Zhang, Y.; Zhang, W.; Schlüter, A. D.; Zenobi, R. Chemical Mapping of Nanodefects within 2d Covalent Monolayers by Tip-Enhanced Raman Spectroscopy. *ACS Nano* **2018**, *12*, 5021−5029.
(65) Mahapatra, S.; Schultz, J. F.; Ning, Y.; Zhang, J.-L.; Jiang, N. Probing Surface Mediated Configurations of Nonplanar Regioisomeric Adsorbates Using Ultrahigh Vacuum Tip-Enhanced Raman Spectroscopy. *Nanoscale* **2019**, *11*, 19877−19883.
(66) Chiang, N.; Jiang, N.; Chulhai, D. V.; Pozzi, E. A.; Hersam, M. C.; Jensen, L.; Seideman, T.; Van Duyne, R. P. Molecular-Resolution Interrogation of a Porphyrin Monolayer by Ultrahigh Vacuum Tip-Enhanced Raman and Fluorescence Spectroscopy. *Nano Lett.* **2015**, *15*, 4114−4120.
(67) Whiteman, P. J.; Schultz, J. F.; Porach, Z. D.; Chen, H.; Jiang, N. Dual Binding Configurations of Subphthalocyanine on Ag(100) Substrate Characterized by Scanning Tunneling Microscopy, Tip-Enhanced Raman Spectroscopy, and Density Functional Theory. *J. Phys. Chem. C* **2018**, *122*, 5489−5495.
(68) Mahapatra, S.; Ning, Y.; Schultz, J. F.; Li, L.; Zhang, J.-L.; Jiang, N. Angstrom Scale Chemical Analysis of Metal Supported Trans- and Cis-Regioisomers by Ultrahigh Vacuum Tip-Enhanced Raman Mapping. *Nano Lett.* **2019**, *19*, 3267−3272.
(69) Zhang, R.; Zhang, X.; Wang, H.; Zhang, Y.; Jiang, S.; Hu, C.; Zhang, Y.; Luo, Y.; Dong, Z. Distinguishing Individual DNA Bases in a Network by Non-Resonant Tip-Enhanced Raman Scattering. *Angew. Chem., Int. Ed.* **2017**, *56*, 5561−5564.

https://doi.org/10.1021/acs.jpcc.2c01434
J. Phys. Chem. C 2022, 126, 8734−8741